Available online at www.sciencedirect.com
ScienceDirect
Trans. Nonferrous Met. Soc. China 33(2023) 3113−3121
Transactions of Nonferrous Metals Society of China
www.tnmsc.cn

Effect of Al_2O_3 insertion layer on ferroelectricity in HfO_2/ZrO_2 nanolaminates

Hai-yan CHEN[1], Yong-hong CHEN[1], Qiu-ju LIANG[2], Zhi-guo WANG[2], Jun CAO[2], Dou ZHANG[1]

1. Powder Metallurgy Research Institute, Central South University, Changsha 410083, China;
2. Technology Center of China Tobacco Hunan Industrial Co., Ltd., Changsha 410007, China

Received 30 April 2022; accepted 4 July 2022

Abstract: Ferroelectric HfO_2 with excellent scaling capability and good complementary-metal-oxide-semiconductor (CMOS) technology compatibility has triggered the interest in nonvolatile memories. Here, $(HfO_2{-}ZrO_2)_3/mAl_2O_3/(HfO_2{-}ZrO_2)_3$ (m donate the Al_2O_3 (AO) thickness) nanolaminates with different AO thicknesses were fabricated using atomic layer deposition method. Ferroelectricity and reliability were investigated by varying AO thickness in the deposition process. The highest remnant polarization (P_r) of 23.87 μC/cm^2 is obtained in $(HZO)_3/1AO/(HZO)_3$ nanolaminate with 1 nm-thick AO dielectric layer. The leakage current can be decreased by 2−3 orders of magnitude with the increase of AO thickness. The performance enhancement is ascribed to the interfacial polarization because of the dielectric mismatch between AO and $HfO_2{-}ZrO_2$ (HZO) and high breakdown strength of AO. The insertion of lower-permittivity AO can effectively modulate the distribution of electric field in nanolaminates and achieves a significant improvement in reliability. Improved ferroelectricity and reliability in ferroelectric/dielectric/ferroelectric structure pave a new way for the designation of HfO_2-based ferroelectric memories with broader thickness range.
Key words: $HfO_2{-}ZrO_2$; nanolaminate; ferroelectricity; reliability; Al_2O_3

1 Introduction

With the development of the Internet of Things, big data, artificial intelligence, non-volatile memory devices with large storage capability, high operation speed and long service life are highly demanded. Ferroelectric materials are strong competitors due to their bi-stable polarization characteristics when the external electric field is removed away [1]. The discovery of ferroelectricity in Si:HfO_2 films has attracted great interest due to simple composition, ultrathin thickness and CMOS compatibility [2]. Numerous investigations on ferroelectric HfO_2-based films have been reported in performance inducement and modulation, structural exploration and probable applications, which breaks the shackles of traditional perovskite materials, such as environmental problems and scaling problems [3−5]. Various methods had been employed to stabilize ferroelectric orthorhombic phase in HfO_2-based film, such as chemical doping [6,7], stress clamping [8,9] and surface energy effect [4,10−12]. Though great progress has been achieved, the reliability problem is still an unresolved issue and the enhancement of ferroelectricity is also a common concern of researchers. It has been proven that HfO_2 [13] and ZrO_2 [14−16] as seed layers can effectively improve the ferroelectric properties of HfO_2-based film. Furthermore, the comprehensive investigations have been performed on the dependence of various parameters including deposition temperatures, individual HfO_2/ZrO_2 layer thickness and deposition sequence of individual layer on the electrical properties of HfO_2/

Corresponding author: Jun CAO, Tel: +86-17608407001, E-mail: caoj0531@hngytobacco.com
DOI: 10.1016/S1003-6326(23)66321-6

ZrO_2 nanolaminates [17−19]. In addition, the introduction of Al_2O_3 with low permittivity as a buffer layer between ferroelectrics and electrodes in $Hf_{0.5}Zr_{0.5}O_2$ films has been reported, which proved that Al_2O_3 is beneficial to improving the reliability of the capacitors [20−22]. Al_2O_3 film is recognized to behave as the capping layer or blocking layer for electron passing and grain growth, which can finally influence the electrical properties of $Hf_{0.5}Zr_{0.5}O_2$ solid solutions.

The above studies are mainly focused on the effect of ferroelectrics/dielectrics (FE/DE) structure on ferroelectric properties. In addition, JAKSCHIK et al [23] reported that 1 nm-thick Al_2O_3 (AO) insertion layer between adjacent $Hf_{0.5}Zr_{0.5}O_2$ films could block the growth of grains and reduce leakage current. SULZBACH et al [24] investigated the contribution of polarization reversal and conducting filaments controlled by grain boundaries on resistive switching, and found that ultrathin crystalline $SrTiO_3$ or amorphous AlO_x capping layers could improve the operation window of HfO_2-based tunnel device through blocking of the ionic channel. A considerable number of reports have been focused on $HfZrO_4$ solid solutions and HfO_2−ZrO_2 superlattices, but few reports have involved in HfO_2−ZrO_2 (HZO) nanolaminates.

In this work, the $(HZO)_3/mAO/(HZO)_3$ nanolaminates were fabricated using atomic layer deposition (ALD) technique through varying the deposition cycling numbers of AO film (m is the AO thickness). In addition, the crystal structure, ferroelectric response and electric field distribution were also investigated. Interfaces and AO interlayers can be adopted to inhibit the growth of nanocrystals and block the development of electrons in HZO nanolaminates, which can promote the enhancement of ferroelectricity and decrease the leakage current. The main purpose of this study is to design a structure of ferroelectric/dielectric/ferroelectric nanolaminates with strong ferroelectricity and low leakage, and develop an understanding of possible reasons for the performance variety.

2 Experimental

2.1 Films deposition

Si substrates were cleaned carefully by reliability change analysis (RCA) cleaning process before using. Bottom electrodes and top electrodes were fabricated through direct-current reactive sputtering technique in the mixture atmosphere of Ar and N_2. Au hard layer was prepared by DC sputtering using a hard mask with a diameter of 300 μm. HZO and Al_2O_3 films were deposited by atomic layer deposition (ALD) method. The complete schematic diagram of preparation sequence in the HZO/AO/HZO nano-laminates is shown in Fig. 1. HZO layer was formed by depositing metal organic precursors tetrakis-ethylmethylamino-hafnium (TEMAH) and tetrakis-ethylmethylamino-zirconium (TEMAZ) at 250 ℃ alternately. Each layer of HZO consists of 12 cycles HfO_2 and 12 cycles ZrO_2. Al_2O_3 was deposited using trimethylaluminium (TMA) at 150 ℃ in chamber. In the whole preparation process, H_2O was used as an oxidizer. All HZO/AO/HZO nanolaminates were annealed in a nitrogen atmosphere at 450 ℃ for 30 s by a rapid thermal annealing (RTA) treatment.

2.2 Materials characterization

The thickness of all films was calculated according to the growth rate of HfO_2, ZrO_2 and Al_2O_3, which were measured to be 0.094, 0.086 and 0.100 nm per cycle by an ellipsometer [19], respectively. The polarization−electric field strength (P−E) loops, current−electric field strength (I−E) loops and leakage current (J−E) curves were performed on an Aix ACCT Systems TF Analyzer 2000. Polarization remnant (P_r) and coercive field (E_c) can be obtained by P−E loops. The crystal structure was investigated using grazing incidence X-ray diffraction (GI-XRD) on a Bruker D8 Advanced system (Cu K_α radiation, λ=0.154 nm) with an incident angle of 1.5° and an integration

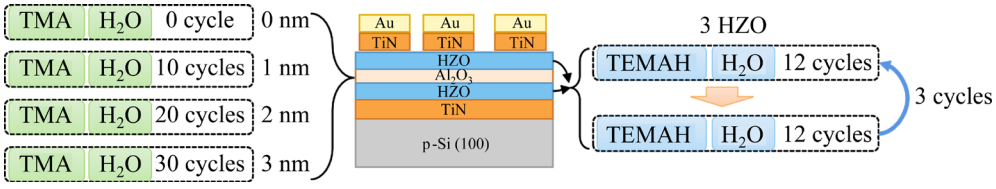

Fig. 1 Schematic diagram of HZO/AO/HZO nanolaminates

time of 2 s per step. The influence of Al_2O_3 thickness on the distribution of electric field in HZO/AO/ HZO nanolaminates was carried out by ANSYS. The piezoelectric response of HZO/AO/ HZO nanolaminates was studied by piezoelectric force microscope (PFM, NanoMan, Veeco). The internal structures were performed to verify the existence of polar *o*-phase by transmission emission microscopy (TEM, Titan G2 60−300, FEI Co., USA) and HRTEM measurement.

3 Results and discussion

3.1 Structure of nanolaminates

Figure 2 shows the GI-XRD pattern of HZO/*m*AO/HZO nanolaminates from 25° to 50° with different AO thickness (0−3 nm). According to the standard PDF card, the diffraction peaks of *o*(111), *t*(001) and *m*(111) are located at 29.863°, 30.063° and 31.669°, respectively. The main peak at 30.5° indicates the coexistence of ferroelectric orthorhombic phase (*o*-phase), tetragonal phase (*t*-phase) and monoclinic phase (*m*-phase) due to their similar lattice parameters [18]. With increasing the thickness of Al_2O_3, the diffraction peak near 30° gradually becomes wide, which can be ascribed to the ultrathin thickness and amorphous characteristic of AO. KATZ et al [25,26] previously reported that ultrathin Al_2O_3 film is amorphous below 6 nm due to its lower surface energy for the less stable non-crystalline phase. Meanwhile, low deposition temperature (150 ℃) and annealing temperature (450 ℃) make AO difficult to crystallize [23]. The *m*-phase with peaks located at 28.3° and 31.7° appears with increasing the thickness of HZO layer.

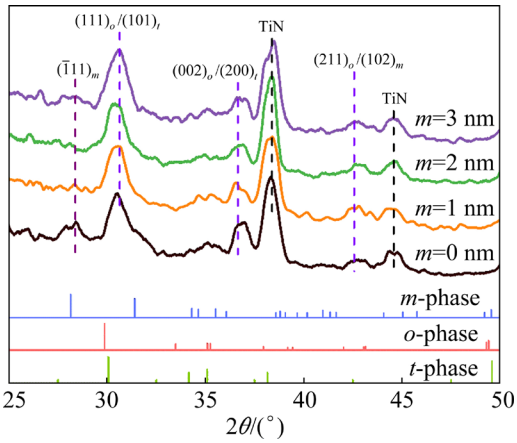

Fig. 2 GI-XRD pattern of $(HZO)_3/mAO/(HZO)_3$ nanolaminates

Grain sizes can be largely increased with film thickness based on previous investigations [19,27]. Larger grain size for thicker films contributes to the growth of *m*-phase because of its lower surface energy. TiN diffraction peaks at 36° and 42° display the good crystallization of electrodes, which can provide large clamping stress for the formation of *o*-phase and promise the good growth quality of ferroelectric films [28,29].

3.2 Ferroelectric performance

Figures 3(a−d) show the polarization−electric field strength (*P*−*E*) loops and current−electric field strength (*I*−*E*) loops of $(HZO)_3/mAO/(HZO)_3$ nanolaminates as a function of AO thickness of 0−3 nm at the applied electric field of 6 MV/cm. The polarization hysteresis displays good rectangularity, indicating their superior ferroelectricity due to domain switching under high electric field. The corresponding *I*−*E* loops also show significant current peaks. The detailed P_r values are as shown in Fig. 3(e). Interestingly, with the insertion of AO layer in the middle layer of HZO, the P_r value increases significantly from 4.99 to 23.87 μC/cm^2 when AO thickness varies from 0 to 1 nm. However, P_r value reduces to 15.49 μC/cm^2 with AO thickness increasing to 3 nm. The large ferroelectricity of the nanolaminate can even be comparable to that in $Hf_{0.5}Zr_{0.5}O_2$ solid solutions [9,30].

The improvement of P_r is attributed to the interfacial polarization and the blocking growth of grain size due to the insertion of lower-permittivity AO compared to HZO [21,31,32]. P_r values are large, which are still much lower than the calculated value (50−53 μC/cm^2) by the ionic distance between Hf^{4+} and O^{2-} in *o*-phase due to the polycrystalline characteristics [33,34]. As shown in Fig. 3(f), E_c shows a decreasing trend monotonously with increasing AO thickness. Large amount of applied electric field can be consumed by AO due to its dielectric characteristic and lower-permittivity (~9) value, which reduces the practical electric field applied on ferroelectric HZO. Thus, larger electric field should be applied on nanolaminates to induce the domain switching.

3.3 Reliability

To further investigate the dependence of AO thickness on the reliability of nanolaminates, the leakage current behaviors are measured, as shown

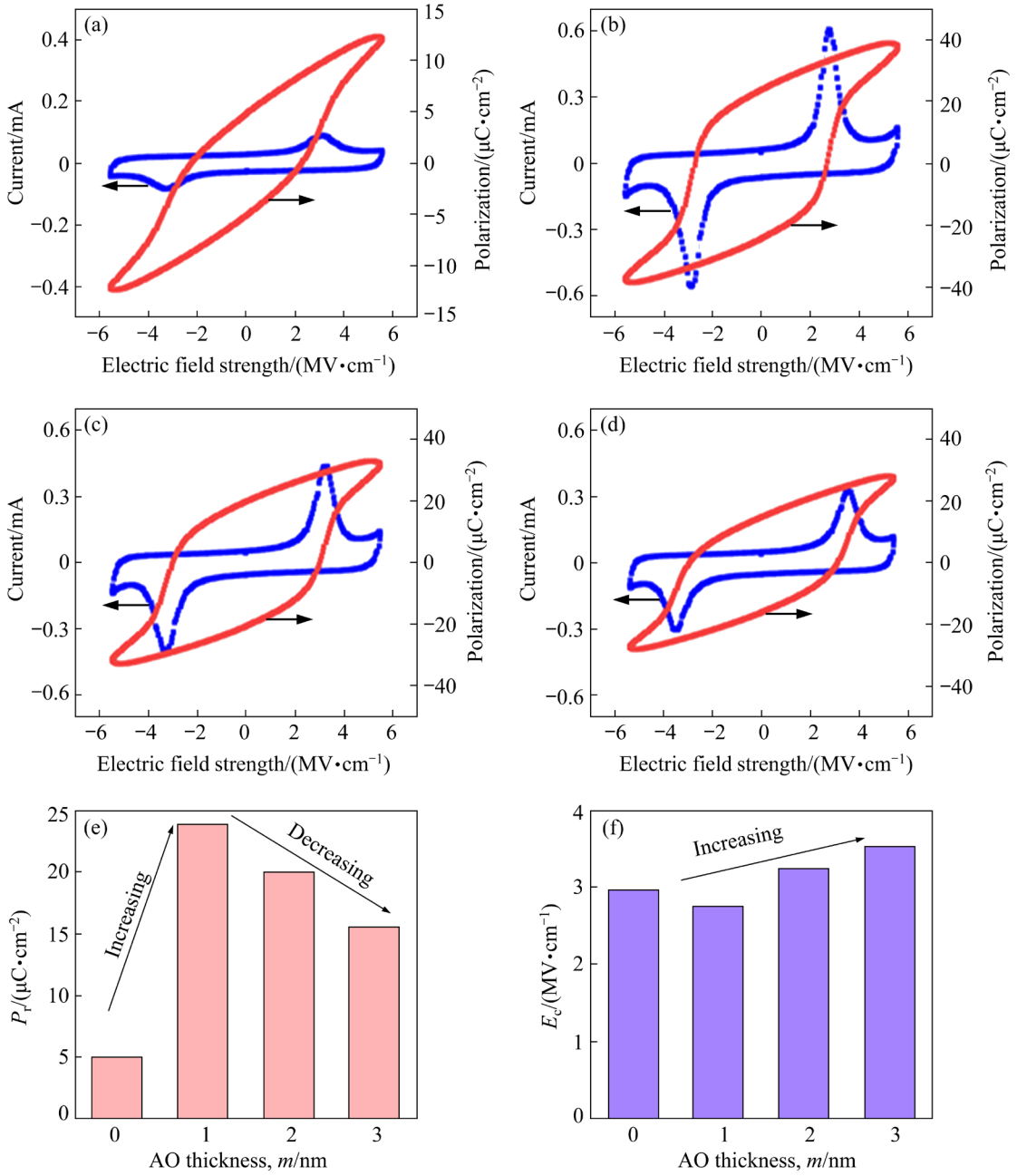

Fig. 3 P−E loops of $(HZO)_3/mAO/(HZO)_3$ nanolaminates with corresponding I−E loops for different AO thickness of m=0 nm (a), m=1 nm (b), m=2 nm (c), and m=3 nm (d), and correlation between P_r (e) and E_c (f) with AO thickness at applied electric field of 6 MV/cm

in Fig. 4(a). The leakage current increases with the increase of applied voltage. The leakage current reduces from 3.13×10^{-2} to 8.67×10^{-3} A/cm^2 for $(HZO)_3/mAO/(HZO)_3$ nanolaminates with m increasing from 0 to 1 nm. AO insertion layer can inhibit the growth of electric tree from HZO films because of its large band width, which avoids the soft or hard breakdown of ferroelectric films [35]. Meanwhile, AO layer can block the continuous grain growth in HZO films and decrease the formation of m-phase, which can be effective in improving the ferroelectric properties of HZO films [36]. The fatigue performance of $(HZO)_3/mAO/(HZO)_3$ nanolaminates with different AO thickness is also characterized at 4 MV/cm, as shown in Fig. 4(b). P_r values decrease continuously with increasing cycles of electric field, which is reported to be caused by the generation of new defects during the process [37]. Slight enhancement of P_r values with AO thickness of 1 nm can be induced by the interfacial polarization, and decreasing fatigue magnitude can be attributed

to its lower electronic carriers in films. When AO thickness is up to 3 nm, the increase of depolarization electric field can exacerbate the instability of nanolaminates and decrease the fatigue performance.

3.4 Simulation

In order to have a deeper understanding on the reliability performance, the electric field distribution of $(HZO)_3/mAO/(HZO)_3$ nanolaminates is analyzed via finite element simulation, as shown in Fig. 5. The permittivities of HfO_2, ZrO_2, and Al_2O_3 are set to be 30, 27 and 10, respectively. The color scale bars indicate the magnitude of the local electric field strength. With the increase of AO thickness, the effective electric field applied on HZO films can be significantly reduced due to the sharing of electric field by lower-k AO films. Much larger effective electric field in AO layer (14.7 MV/cm with m=1 nm) is due to the permittivity difference from HZO layer. From above results, the insertion of AO film can share most of the applied electric field and decrease the practical field in HZO nanolaminates, and finally

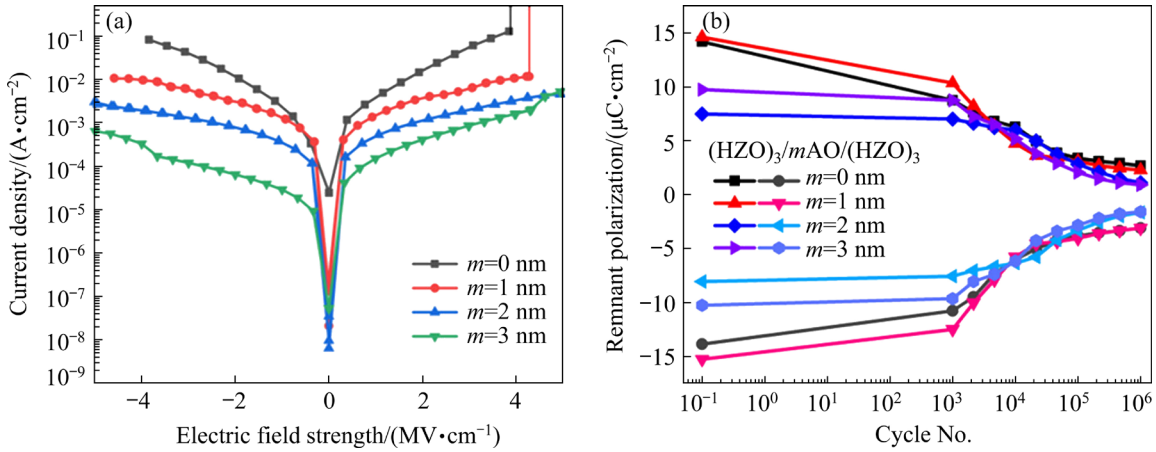

Fig. 4 J−E curves under applied voltage of 0−5 MV/cm (a) and fatigue performance of $(HZO)_3/mAO/(HZO)_3$ nanolaminates

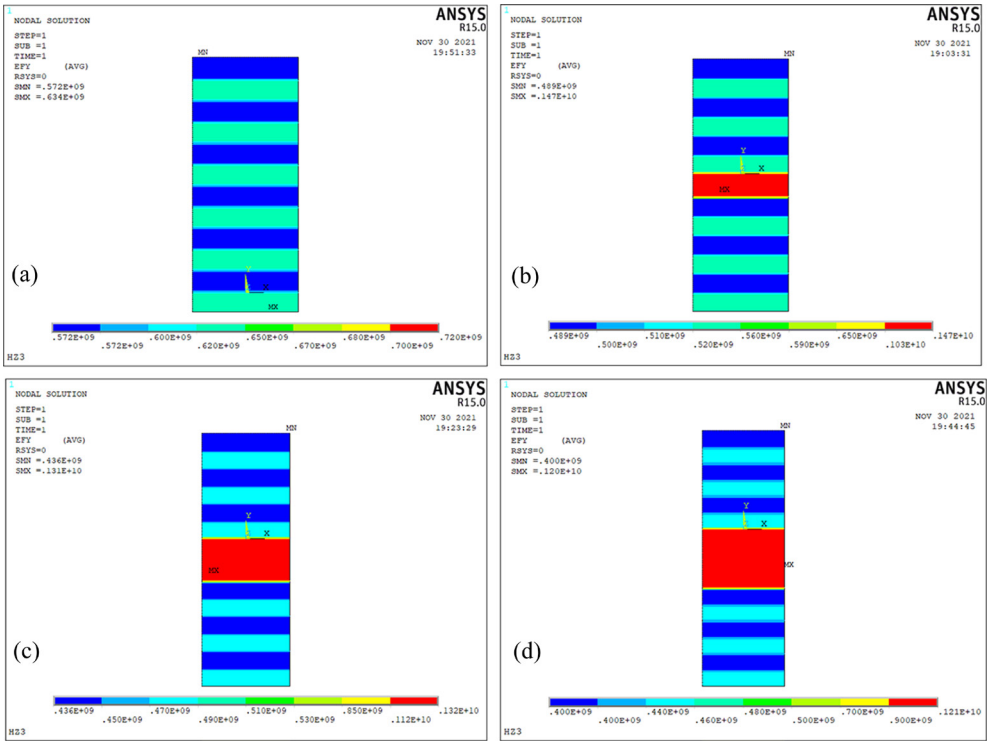

Fig. 5 Electric filed strength distribution of $(HZO)_3/mAO/(HZO)_3$ nanolaminates: (a) m=0 nm; (b) m=1 nm; (c) m=2 nm; (d) m=3 nm

decrease the leakage current in multilayered films. Thus, larger electric field should be applied to making ferroelectric switching, which leads to the increase of coercive fields. These results can well explain the decrease of leakage current with an AO insertion layer, as shown in Fig. 4(a). The applied electric field on each film can be decreased with the increase of its permittivity according to the equal charge quantity in series capacitors [38]. Therefore, under the same electric field, the insertion of the Al_2O_3 layer can effectively reduce the possibility of breakdown and failure of the HZO layer, which contributes to the better reliability.

3.5 Phase structure of $(HZO)_3$/1AO/$(HZO)_3$

Figure 6(a) shows the PFM images with obvious "box-in-box" pattern under the sample bias of 8 V, which can clarify the origins of ferroelectricity in $(HZO)_3$/1AO/$(HZO)_3$ nanolaminates. The center area of 3.6 μm × 3.6 μm was polarized by a positive tip bias of +8 V, and then a smaller square of 1.8 μm × 1.8 μm was polarized negatively by a tip bias of −8 V. The outer area of 6 μm × 6 μm was obtained without sample bias. The significant contrasts of unpolarized, positively polarized and negatively polarized regions are clearly displayed under different directional sample bias, which indicates the nature of piezoelectric response in ferroelectric films through domain switching [39]. Figures 6(b, c) show the local amplitude loops with corresponding phase hysteresis loops of $(HZO)_3$/1AO/$(HZO)_3$ nanolaminates under the sample bias of 8 V. Typical butterfly curves can be seen and the maximum amplitude can reach 33.2 mV. And nearly 180° phase difference reveals the internal ferroelectricity of nanolaminates. The slightly different positive and negative coercive voltage during PFM tests is attributed to the built-in field, which is caused by the different interfacial conditions.

The cross-sectional image of $(HZO)_3$/1AO/HZO_3 nanolaminates is characterized by TEM, as shown in Fig. 6(d). The interfacial layer between TiN electrode and the film can be significantly displayed due to the oxidation of TiN with its exposure to atmosphere [40]. The high-resolution transmission emission microscopy (HRTEM) is performed on the film to further verify the internal structures, as shown in Figs. 6(e, f). The significant polycrystalline characteristics are shown with the coexistence of *m*-phase, *t*-phase and polar *o*-phase from the lattice fringes. The *d*-spacings of $(111)_o$, $(200)_o$ and $(022)_o$ are 2.99, 2.70 and 1.84 Å,

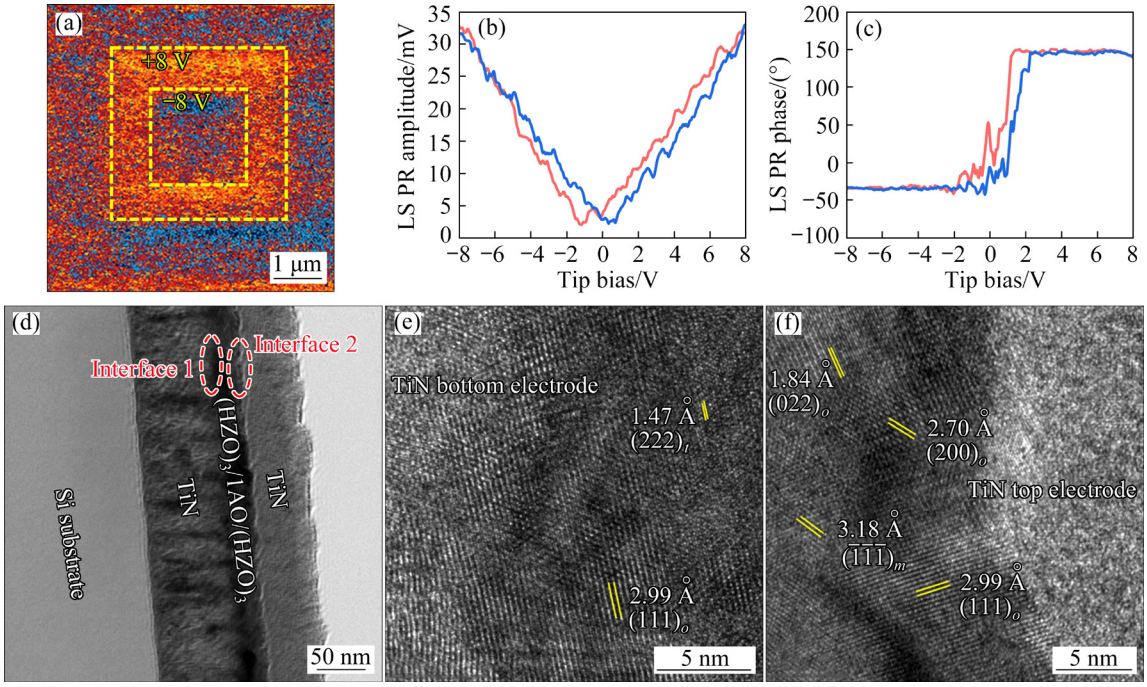

Fig. 6 PFM image with "box-in-box" pattern under DC biases of 8 V (a); Local amplitude loops (b) and phase hysteresis loops (c) for $(HZO)_3$/1AO/$(HZO)_3$ nanolaminates; Cross-sectional image of TiN/$(HZO)_3$/1AO/$(HZO)_3$/TiN sample (d); Interface 1 between TiN bottom electrode and HZO nanolaminates (e), and Interface 2 between TiN top electrode and HZO nanolaminates (f)

respectively, which match well with the GIXRD results as shown in Fig. 2(b) and previous reports. The calculated crystal orientations represent the asymmetric structures of the sample. The insertion of 1 nm-thick Al_2O_3 middle layer cannot influence the basic structure of $(HZO)_3/1AO/(HZO)_3$ nano-laminates [21,41,42]. The lattice fringes near top electrode can be clearer compared to that near bottom electrode, which is attributed to the clamping stress by TiN top electrode.

4 Conclusions

(1) $(HZO)_3/m$AO$/(HZO)_3$ nanolaminates with robust ferroelectricity and excellent reliability were successfully fabricated using ALD method.

(2) The ferroelectricity is optimized by adjusting both HZO deposition cycle and Al_2O_3 thickness. Large P_r of 23.87 μC/cm^2 is obtained in $(HZO)_3/1AO/(HZO)_3$ nanolaminates. The leakage current can be effectively decreased by one order of magnitude when the insertion thickness of AO is 1 nm at the electric field of 1 MV/cm.

(3) The distribution of electric field is simulated by ANSYS, which indicates the successful sharing of the applied electric field. This work unfolds the flexibility of the ferroelectric/dielectric/ferroelectric structure to adjust the ferroelectric properties, which provides a feasible method for the designing and fabrication of relevant ferroelectric devices.

Acknowledgments

This research was financially supported by the National Key R&D Program of China (No. 2021YFB2012100), the National Natural Science Foundation of China (Nos. U19A2087, 52172134), the Construction of Innovative Provinces in Hunan Province, China (No. 2020GK2062), and the State Key Laboratory of Powder Metallurgy, Central South University, China.

References

[1] IHLEFELD J F. Ferroelectricity in doped hafnium oxide: Materials, properties and devices [M]. Sawston, Cambridge: Woodhead, 2019: 1−24.

[2] BÖSCKE T S, MÜLLER J, BRÄUHAUS D, SCHRÖDER U, BÖTTGER U. Ferroelectricity in hafnium oxide thin films [J]. Applied Physics Letters, 2011, 99(10): 102903.

[3] PESIC M, SCHROEDER U, SLESAZECK S, MIKOLAJICK T. Comparative study of reliability of ferroelectric and anti-ferroelectric memories [J]. IEEE Transactions on Device and Materials Reliability, 2018, 18(2): 154−162.

[4] PARK M H, LEE Y H, KIM H J, KIM Y J, MOON T, KIM K D, MULLER J, KERSCH A, SCHROEDER U, MIKOLAJICK T, HWANG C S. Ferroelectricity and antiferroelectricity of doped thin HfO_2-based films [J]. Advanced Materials, 2015, 27(11): 1811−1831.

[5] GRIMLEY E D, SCHENK T, SANG X, PEŠIĆ M, SCHROEDER U, MIKOLAJICK T, LEBEAU J M. Structural changes underlying field-cycling phenomena in ferroelectric HfO_2 thin films [J]. Advanced Electronic Materials, 2016, 2(9): 1600173.

[6] PARK M H, SCHENK T, FANCHER C M, GRIMLEY E D, ZHOU C, RICHTER C, LEBEAU J M, JONES J L, MIKOLAJICK T, SCHROEDER U. A comprehensive study on the structural evolution of HfO_2 thin films doped with various dopants [J]. Journal of Materials Chemistry C, 2017, 5(19): 4677−4690.

[7] MATERLIK R, KÜNNETH C, FALKOWSKI M, MIKOLAJICK T, KERSCH A. Al-, Y-, and La-doping effects favoring intrinsic and field induced ferroelectricity in HfO_2: A first principles study [J]. Journal of Applied Physics, 2018, 123(16): 164101.

[8] RYU H, XU K, KIM J, KANG S, GUO J, ZHU W. Exploring new metal electrodes for ferroelectric aluminum-doped hafnium oxide [J]. IEEE Transactions on Electron Devices, 2019, 66(5): 2359−2364.

[9] KIM H, KASHIR A, OH S, HWANG H. A new approach to achieving strong ferroelectric properties in TiN/$Hf_{0.5}Zr_{0.5}O_2$/TiN devices [J]. Nanotechnology, 2021, 32(5): 055703.

[10] CHEEMA S S, KWON D, SHANKER N, DOS REIS R, HSU S L, XIAO J, ZHANG H, WAGNER R, DATAR A, MCCARTER M R, SERRAO C R, YADAV A K, KARBASIAN G, HSU C H, TAN A J, WANG L C, THAKARE V, ZHANG X, MEHTA A, KARAPETROVA E, CHOPDEKAR R V, SHAFER P, ARENHOLZ E, HU C, PROKSCH R, RAMESH R, CISTON J, SALAHUDDIN S. Enhanced ferroelectricity in ultrathin films grown directly on silicon [J]. Nature, 2020, 580(7804): 478−482.

[11] MATERLIK R, KUENNETH C, KERSCH A. The origin of ferroelectricity in $Hf_{1-x}Zr_xO_2$: A computational investigation and a surface energy model [J]. Journal of Applied Physics, 2015, 117(13): 134109.

[12] WEI Y, NUKALA P, SALVERDA M, MATZEN S, ZHAO H J, MOMAND J, EVERHARDT A S, AGNUS G, BLAKE G R, LECOEUR P, KOOI B J, INIGUEZ J, DKHIL B, NOHEDA B. A rhombohedral ferroelectric phase in epitaxially strained $Hf_{0.5}Zr_{0.5}O_2$ thin films [J]. Nature Materials, 2018, 17(12): 1095−1100.

[13] GADDAM V, DAS D, JEON S. Insertion of HfO_2 seed/dielectric layer to the ferroelectric HZO films for heightened remanent polarization in MFM capacitors [J]. IEEE Transactions on Electron Devices, 2020, 67(2): 745−750.

[14] XIAO W, LIU C, PENG Y, ZHENG S, FENG Q, ZHANG C, ZHANG J, HAO Y, LIAO M, ZHOU Y. Performance improvement of $Hf_{0.5}Zr_{0.5}O_2$-based ferroelectric-field-effect transistors with ZrO_2 seed layers [J]. IEEE Electron Device

Letters, 2019, 40(5): 714−717.

[15] YI S H, LIN B T, HSU T Y, SHIEH J, CHEN M J. Modulation of ferroelectricity and antiferroelectricity of nanoscale ZrO_2 thin films using ultrathin interfacial layers [J]. Journal of the European Ceramic Society, 2019, 39(14): 4038−4045.

[16] ONAYA T, NABATAME T, SAWAMOTO N, OHI A, IKEDA N, NAGATA T, OGURA A. Improvement in ferroelectricity of $Hf_xZr_{1-x}O_2$ thin films using top- and bottom-ZrO_2 nucleation layers [J]. APL Materials, 2019, 7(6): 061107.

[17] PARK M H, KIM H J, LEE G, PARK J, LEE Y H, KIM Y J, MOON T, KIM K D, HYUN S D, PARK H W, CHANG H J, CHOI J H, HWANG C S. A comprehensive study on the mechanism of ferroelectric phase formation in hafnia−zirconia nanolaminates and superlattices [J]. Applied Physics Reviews, 2019, 6(4): 041403.

[18] WEEKS S L, PAL A, NARASIMHAN V K, LITTAU K A, CHIANG T. Engineering of ferroelectric HfO_2−ZrO_2 nanolaminates [J]. ACS Applied Materials & Interfaces, 2017, 9(15): 13440−13447.

[19] CHEN Y H, WANG L, LIU L Y, TANG L, YUAN X, CHEN H Y, ZHOU K C, ZHANG D. Thickness-dependent ferroelectric properties of HfO_2/ZrO_2 nanolaminates using atomic layer deposition [J]. Journal of Materials Science, 2021, 56(10): 6064−6072.

[20] WANG J, WANG D, LI Q, ZHANG A, GAO D, GUO M, FENG J, FAN Z, CHEN D, QIN M, ZENG M, GAO X, ZHOU G, LU X, LIU J M. Excellent ferroelectric properties of $Hf_{0.5}Zr_{0.5}O_2$ thin films induced by Al_2O_3 dielectric layer [J]. IEEE Electron Device Letters, 2019, 40(12): 1937−1940.

[21] CHEN H Y, TANG L, LIU L Y, CHEN Y H, LUO H, YUAN X, ZHANG D. Significant improvement of ferroelectricity and reliability in $Hf_{0.5}Zr_{0.5}O_2$ films by inserting an ultrathin Al_2O_3 buffer layer [J]. Applied Surface Science, 2021, 542: 148737.

[22] KIM H J, PARK M H, KIM Y J, LEE Y H, JEON W, GWON T, MOON T, KIM K D, HWANG C S. Grain size engineering for ferroelectric $Hf_{0.5}Zr_{0.5}O_2$ films by an insertion of Al_2O_3 interlayer [J]. Applied Physics Letters, 2014, 105(19): 102903.

[23] JAKSCHIK S, SCHROEDER U, HECHT T, GUTSCHE M, SEIDL H, BARTHA J W. Crystallization behavior of thin ALD-Al_2O_3 films [J]. Thin Solid Films, 2003, 425(1/2): 216−220.

[24] SULZBACH M C, ESTANDIA S, GAZQUEZ J, SANCHEZ F, FINA I, FONTCUBERTA J. Blocking of conducting channels widens window for ferroelectric resistive switching in interface-engineered $Hf_{0.5}Zr_{0.5}O_2$ tunnel devices [J]. Advanced Functional Materials, 2020, 30(32): 2002638.

[25] PROKES S M, KATZ M B, TWIGG M E. Growth of crystalline Al_2O_3 via thermal atomic layer deposition: Nanomaterial phase stabilization [J]. APL Materials, 2014, 2(3): 032105.

[26] KATZ M B, TWIGG M E, PROKES S M. Formation and stability of crystalline and amorphous Al_2O_3 layers deposited on Ga_2O_3 nanowires by atomic layer epitaxy [J]. Journal of Applied Physics, 2016, 120(12): 124311.

[27] KIM H J, PARK M H, KIM Y J, LEE Y H, JEON W, GWON T, MOON T, KIM K D, HWANG C S. Grain size engineering for ferroelectric $Hf_{0.5}Zr_{0.5}O_2$ films by an insertion of Al_2O_3 interlayer [J]. Applied Physics Letters, 2014, 105(19): 192903.

[28] LOMENZO P D, ZHAO P, TAKMEEL Q, MOGHADDAM S, NISHIDA T, NELSON M, FANCHER C M, GRIMLEY E D, SANG X, LEBEAU J M, JONES J L. Ferroelectric phenomena in Si-doped HfO_2 thin films with TiN and Ir electrodes [J]. Journal of Vacuum Science & Technology B, 2014, 32(3): 03d123.

[29] SHIRAISHI T, KATAYAMA K, YOKOUCHI T, SHIMIZU T, OIKAWA T, SAKATA O, UCHIDA H, IMAI Y, KIGUCHI T, KONNO T J, FUNAKUBO H. Impact of mechanical stress on ferroelectricity in $Hf_{0.5}Zr_{0.5}O_2$ thin films [J]. Applied Physics Letters, 2016, 108(26): 262904.

[30] SCHROEDER U, RICHTER C, PARK M H, SCHENK T, PESIC M, HOFFMANN M, FENGLER F P G, POHL D, RELLINGHAUS B, ZHOU C, CHUNG C C, JONES J L, MIKOLAJICK T. Lanthanum-doped hafnium oxide: a robust ferroelectric material [J]. Inorganic Chemistry, 2018, 57(5): 2752−2765.

[31] ROYTBURD A L, ZHONG S, ALPAY S P. Dielectric anomaly due to electrostatic coupling in ferroelectric−paraelectric bilayers and multilayers [J]. Applied Physics Letters, 2005, 87(9): 092902.

[32] LIU Y, PENG X P. Electrostatic coupling with interfacial free charge in ferroelectric–paraelectric bilayers and superlattices [J]. Physics Letters A, 2011, 375(45): 4091−4094.

[33] JONES J L. The effect of crystal symmetry on the maximum polarization of polycrystalline ferroelectric materials [J]. Materials Science and Engineering B−Advanced Functional Solid-State Materials, 2010, 167(1): 6−11.

[34] CLIMA S, WOUTERS D J, ADELMANN C, SCHENK T, SCHROEDER U, JURCZAK M, POURTOIS G. Identification of the ferroelectric switching process and dopant-dependent switching properties in orthorhombic HfO_2: A first principles insight [J]. Applied Physics Letters, 2014, 104(9): 092906.

[35] CHOI H S, LIM G S, LEE J H, KIM Y T, KIM S I, YOO D C, LEE J Y, CHOI I H. Improvement of electrical properties of ferroelectric gate oxide structure by using Al_2O_3 thin films as buffer insulator [J]. Thin Solid Films, 2003, 444(1/2): 276−281.

[36] KIM H J, PARK M H, KIM Y J, LEE Y H, JEON W, GWON T, MOON T, DO KIM K, HWANG C S. Grain size engineering for ferroelectric $Hf_{0.5}Zr_{0.5}O_2$ films by an insertion of Al_2O_3 interlayer [J]. Applied Physics Letters, 2014, 105(19): 192903.

[37] HUANG F, CHEN X, LIANG X, QIN J, ZHANG Y, HUANG T, WANG Z, PENG B, ZHOU P, LU H, ZHANG L, DENG L, LIU M, LIU Q, TIAN H, BI L. Fatigue mechanism of yttrium-doped hafnium oxide ferroelectric thin films fabricated by pulsed laser deposition [J]. Physical Chemistry Chemical Physics, 2017, 19(5): 3486−3497.

[38] LUO H, ZHOU X F, ELLINGFORD C, ZHANG Y, CHEN S, ZHOU K C, ZHANG D, BOWEN C R, WAN C Y. Interface design for high energy density polymer nanocomposites [J].

Chemical Society Reviews, 2019, 48(16): 4424−4465.
[39] STRELCOV E, KIM Y, YANG J C, CHU Y H, YU P, LU X, JESSE S, KALININ S V. Role of measurement voltage on hysteresis loop shape in piezoresponse force microscopy [J]. Applied Physics Letters, 2012, 101(19): 192902.
[40] MITTMANN T, MATERANO M, CHANG S C, KARPOV I, MIKOLAJICK T, SCHROEDER U. Impact of oxygen vacancy content in ferroelectric HZO films on the device performance [C]//Proceedings of IEDM 2020. Electronic Network: IEEE, 2020: 11−14.
[41] KANG H K, KANG Y S, BAIK M, JEONG K S, KIM D K, SONG J D, CHO M H. Improving electrical properties by effective sulfur passivation via modifying the surface state of substrate in HfO_2/InP systems [J]. Journal of Physical Chemistry C, 2018, 122(13): 7226−7235.
[42] ZHENG X J, ZHANG J J, ZHOU Y C, TANG M H, YANG B, CHEN Y Q. Simulation of electric properties of MFIS capacitor with BNT ferroelectric thin film using Silvaco/Atlas [J]. Transactions of Nonferrous Metals Society of China, 2007, 17(Suppl.): 752−755.

Al_2O_3 插入层对 HfO_2/ZrO_2 叠层薄膜铁电性能的影响

陈海燕[1]，陈永红[1]，梁秋菊[2]，王志国[2]，曹 俊[2]，张 斗[1]

1. 中南大学 粉末冶金研究院，长沙 410083；
2. 湖南中烟工业有限责任公司 技术中心，长沙 4100007

摘 要：基于优良的可扩展性和良好的互补金属氧化物半导体工艺兼容性，铁电 HfO_2 基非易失性存储器引发广泛的研究兴趣。采用原子层沉积方法制备$(HfO_2–ZrO_2)_3/mAl_2O_3/(HfO_2–ZrO_2)_3$ 纳米叠层薄膜(m 为 Al_2O_3 厚度)，并通过改变 Al_2O_3 厚度研究其铁电性和可靠性。结果表明，当 m 为 1 nm 时，叠层薄膜表现出最高的剩余极化值，为 23.87 μC/cm^2，且随着 Al_2O_3 厚度的增加，漏电流值可降低 2−3 个数量级。Al_2O_3 和 $HfO_2–ZrO_2$ 因介电错配而产生界面极化，同时更低介电常数的 Al_2O_3 可有效调控叠层薄膜内部的电场分布，从而促进铁电性能和可靠性的协同提升，这为更宽厚度范围 HfO_2 基铁电存储器件的设计提供新的思路。

关键词：$HfO_2–ZrO_2$；纳米叠层；铁电性；可靠性；Al_2O_3

(Edited by Bing YANG)